DTU Library

Insights into Kinetics of Methane Hydrate Formation in the Presence of Surfactants

Pandey, Jyoti Shanker; Jouljamal Daas, Yousef ; Solms, Nicolas von

Link back to DTU Orbit

Article

Insights into Kinetics of Methane Hydrate Formation in the Presence of Surfactants

Jyoti Shanker Pandey, Yousef Jouljamal Daas and Nicolas von Solms *

Center for Energy Resource Engineering (CERE), Department of Chemical Engineering,
Technical University of Denmark, 2800 Lyngby, Denmark

* Correspondence: nvs@kt.dtu.dk; Tel.: +45-4525-2867

Abstract: Sodium dodecyl sulfate (SDS) is a well-known surfactant, which can accelerate methane hydrate formation. In this work, methane hydrate formation kinetics were studied in the presence of SDS using a rocking cell apparatus in both temperature-ramping and isothermal modes. Ramping and isothermal experiments together suggest that SDS concentration plays a vital role in the formation kinetics of methane hydrate, both in terms of induction time and of final gas uptake. There is a trade-off between growth rate and gas uptake for the optimum SDS concentration, such that an increase in SDS concentration decreases the induction time but also decreases the gas storage capacity for a given volume. The experiments also confirm the potential use of the rocking cell for investigating hydrate promoters. It allows multiple systems to run in parallel at similar experimental temperature and pressure conditions, thus shortening the total experimentation time. Understanding methane hydrate formation and storage using SDS can facilitate large-scale applications such as natural gas storage and transportation.

Keywords: methane hydrate; rocking cell; sodium dodecyl sulfate; induction time; gas uptake

1. Introduction

Methane hydrate formation is an area of interest for many applications, such as natural gas storage and transport [1,2] and as a potential hydrocarbon resource from hydrate-bearing sediments [3,4] and CH_4-CO_2 replacement [5]. These applications require the formation of hydrates in bulk water or hydrates in sediments in the laboratory. There are two main methods suggested to improve hydrate growth rate: One is mechanical, and the other is chemical. In the mechanical method, stirring [6] and nozzle spray [7] are common practice, while in the chemical method, thermodynamic [8] and kinetic promoters [9,10] are considered, which could lead to enhanced mass transfer between gas and liquid to accelerate the hydrate formation.

Surfactants are popular chemicals in petrochemical and food industries due to their ability to modify surface properties. It is well established that the use of surfactants enhances the gas hydrate formation kinetics, and they have been widely investigated at laboratory scale. Two key parameters of surfactants are the Krafft point [11] and critical micelle concentration (CMC) [11], which are generally used to classify surfactant behavior. The Krafft point is the temperature above which surfactant solubility increases sharply. Furthermore, above the Krafft point and the CMC, micelle formation occurs, and reduction in surface tension begins. Surfactants do not form micelles below the CMC, and at the Krafft point the solubility of surfactant is its CMC. Zhang et al. [12] suggested that the Krafft point of SDS does not change under hydrate forming conditions. Hence, the low CMC of SDS is considered responsible for enhancing methane hydrate formation. Song et al. [13] have suggested the contact force, interfacial tension, and adhesion energy decrease as SDS concentration increases for cyclopentane hydrate. Further, Demissie et al. [14] have shown that below the CMC of

SDS, absorption and surface tension decrease, while above the CMC, absorption increases although surface tension remains constant. They also suggested that below the CMC, mainly monomers and some dimers and trimers are present. Above the CMC, micelles are formed with a variety of shapes such as spherical, ellipsoidal, or large rod-like structures. At very high concentration, liquid crystals start to aggregate.

Okutani et al. [9] have suggested that at 1000 ppm and above, SDS is found to enhance the hydrate formation rate and saturation. As per Yoslim et al. [15], a concentration between 240 to 2200 ppm leads to 14 times higher gas uptake for a methane and propane gas mixture, in comparison to the pure water case. Zhang et al. [16] have confirmed the SDS hydrate promotion effect but did not find any systematic trend between concentration and induction time. Additionally, most of the methane hydrate formation studies in the presence of SDS have been done above the ice melting point. Liu et al. [17] have studied the methane hydrate kinetics in the presence of ice particles and below the ice melting point. They concluded that temperature and SDS concentration play an important role in methane hydrate kinetics below the ice melting temperature. However, there is still ambiguity regarding the role of surfactants, the exact mechanisms behind surfactants as promoters, and the optimal concentration for a particular system, such as methane hydrate [18].

Methane hydrate formation kinetics are mostly studied in terms of induction time and gas uptake profile inside a high-pressure cell. There are also studies in which differential scanning calorimeter (DSC) [19,20] is used for nucleation and growth kinetics, and optical microscopy (OM) and Fourier transform infrared spectroscopy in attenuated total reflection mode (ATR-FTIR) [21] are used to study the methane hydrate kinetics. Unfortunately, the application of a rocking cell to study hydrate promoter effects on gas kinetics is found to be very rare.

The rocking cell apparatus has been in use for several years, and different parameters, such as rocking angle, rocking speed, aqueous volume, steel versus glass balls, isothermal versus constant cooling test, cooling rate, kinetic hydrate inhibitor (KHI) performance, and standard operating conditions, have been described in detail by Astrid et al. [22] It is common practice to study gas hydrate kinetics in the presence of promoter using stirred and a non-stirred high-pressure cell and autoclave that come in different configurations along with their cooling baths. Therefore, setup design limits the number of experiments and pressure–temperature (P–T) conditions within the same period. To shorten the experimental timeline, the rocking cell setup has been adopted as an alternative to upscale the investigation. In every rocking cell setup, multiple rocking cells are placed within the same bath, and every rocking cell is a standalone, high-pressure cell. The rocking cell is different from a conventional high-pressure cell in terms of agitation by rocking instead by stirring. Each rocking cell contains a steel or glass ball and is rocked back and forth to create turbulence and mixing of fluid to enhance the hydrate formation. The main advantages of the rocking cell over the conventional high-pressure cell are that several parallel experiments can be run in identical P–T conditions. A standard rocking cell setup will also provide the opportunity to compare data from different research groups. According to Sa et al. [23], key characteristics of the rocking cell are a batch system, which allows for limited mixing; a small volume of the sample used, helping in measurement of gas consumed to run multiple cells in parallel; and the rolling ball, which can give a rough estimate of relative viscosity.

The primary objective of this work is to study the kinetics of the methane hydrate in the presence of sodium dodecyl sulfate (SDS) and to investigate the effects of SDS concentration on different properties such as nucleation temperature, induction time, gas uptake and hydrate saturation using rocking cell. The rocking cell has traditionally been used to study hydrate inhibitors, and in this work we have shown the potential application of rocking cell to evaluate the performance of hydrate promoter in terms of concentration (500–3000 ppm) for methane gas hydrate formation.

2. Materials and Methods

2.1. Material

In this work, methane gas hydrate formation is studied using a rocking cell setup. An analytical grade of methane (99.99%) purity is obtained from Air Liquide. A schematic layout of a rocking cell and detailed setup description is given elsewhere [24,25], while SDS is supplied from Sigma Aldrich. Distilled water is utilized to prepare all the samples by minimizing the effect of impurities in the solution phase.

2.2. Methods

A rocking cell with five identical pressure test cells (RC-5, PSL Systemtechnik, Osterode am Harz, Germany) is used to test the effect of SDS on methane hydrate promotion. Two different temperature programs, constant ramping and isothermal, are applied in this study. Constant ramping experiments are performed at different operating pressures (between 50–120 bar) under a given ramping scheme (15–3 °C in 12 h) to determine onset temperature(T_0) and rapid hydrate formation temperature (T_a) for different concentrations (500 ppm–3000 ppm). Slow constant cooling method allows to evaluate sub cooling requirement before the hydrate start forming using hydrate promoters. Isothermal experiments are performed at constant temperature schemes (3 °C and 5 °C) and at constant operating pressure (90 bar) to evaluate the induction time (t_0), growth rate (K_p), methane gas uptake(n_{CH4}), and hydrate saturation(S_H) for different SDS concentrations. Astrid et al. [22] has suggested that smaller deviation are observed in T_0 value coming from constant cooling experiment than induction time (t_0) observed in isothermal experiments.

The constant ramping test procedure is as follows. (1) Each cell is loaded with 10 mL of SDS solution with different concentration. (2) Air inside each cell is removed via purging the cell with 3–5 bar of methane gas. (3) The cell is pressurized with methane at desire pressure at 25 °C temperature and rocked at 20 rocks per min with a rocking angle of 35°. (4) The cells are cooled further from 25 °C to 15 °C in 1 h and 15 °C to 3 °C in 12 h at a rate of 1 °C/h under flow conditions. (5) The pressure and temperature of each cell and cooling bath are continuously monitored, by a data acquisition (DAQ) system throughout the experiments.

The isothermal test procedure is as follows. (1) Each cell with sample is placed inside the bath and air inside the cell is removed via purging the cell. (2) Temperature of the bath is reduced to experimental pressure of 3 °C and 5 °C. (3) Once the desired temperature is achieved, cells are pressurized with methane at desired pressure of 90 bar. (4) Rocking is started at 20 rocks per min, and 35° angle, and the pressure and temperature of each cell and cooling bath is continuously monitored by DAQ. Each test cell has a volume of 40.13 cm³ and is capable of operating up to 20 MPa.

Hydrate nucleation and formation is a probabilistic event; however, the presence of a hydrate promoter (e.g., SDS) reduces the stochastic nature of hydrate formation, which leads to good reproducibility of the results. In this study, two repetitions per experiment are performed, and results are collected for fresh and memory samples. All the reported values are the average values based on two repetitions.

2.3. Experimental Data Processing

The results from a temperature ramping experiment are shown in Figure 1 In constant ramping mode, initial pressure reduction is due to thermal contraction and due to methane dissolved in SDS solution. At the beginning of hydrate nucleation, pressure and temperature follow linear correlation, and the onset of nucleation is observed from the point where sudden deviation from the linear trend is observed, as shown in Figure 1 These P–T data are plotted against time to detect the formation of methane hydrate, although nucleation is not detectable and may have occurred earlier. Figure 2 shows the P–T graph for one single test cell after constant ramping experiment and methodology to calculate T_0 and T_a. As shown in Figure 3, after approximately 325 min, hydrate formation is observed to occur at 10.5 °C. This point is called onset nucleation temperature T_o, and the steepest

point in the P–T graph occurs at 360 min and 9.8 °C, indicating that the temperature where the most rapid formation of hydrate formation occurs is represented by T_a, determined from the steepest section of the pressure versus time curve.
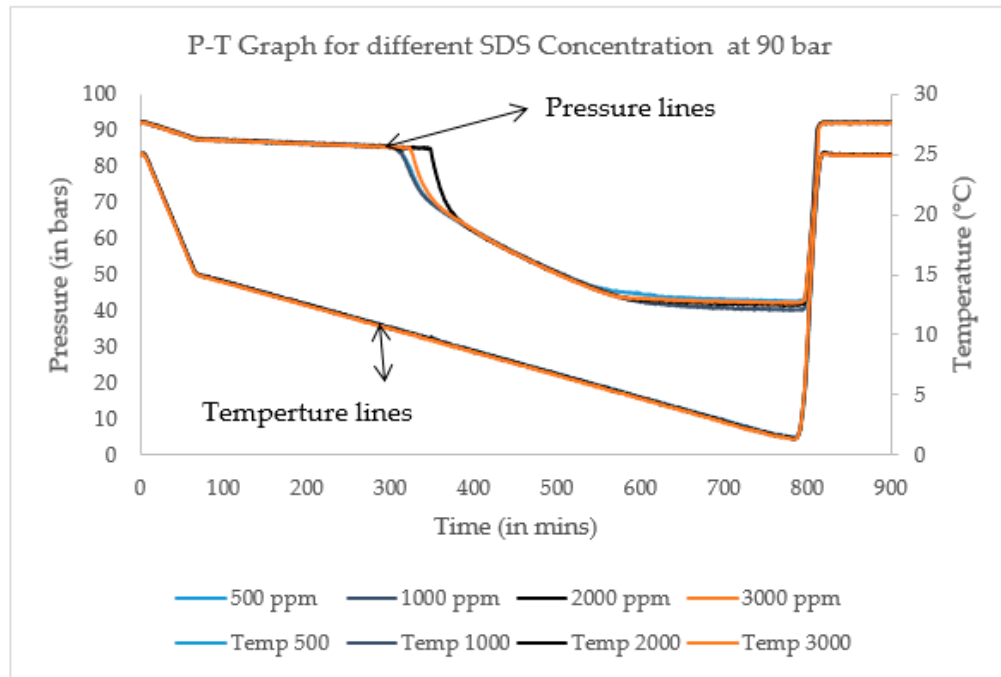

Figure 1. Rocking cell experiment showing pressure and temperature as a function of time during a constant ramping run for four cells. Each cell contains different SDS concentrations (500 ppm to 3000 ppm) (fresh). Initial pressure is 90 bar while temperature ramping started from $T = 15$ °C to 3 °C in 12 h. As the temperature decreases hydrate formation is shown as a sudden drop in pressure. Upon rapid temperature increase, hydrates decompose and the pressure is fully recovered.
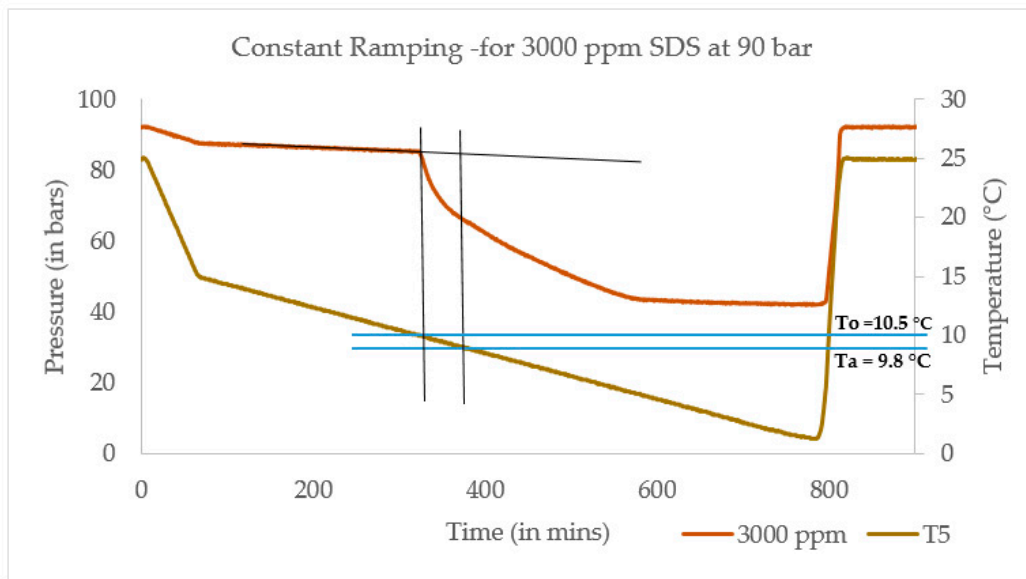

Figure 2. Graphical representation demonstrating typical method to determine T_0 and T_a with P–T graph generated from constant cooling experiment.
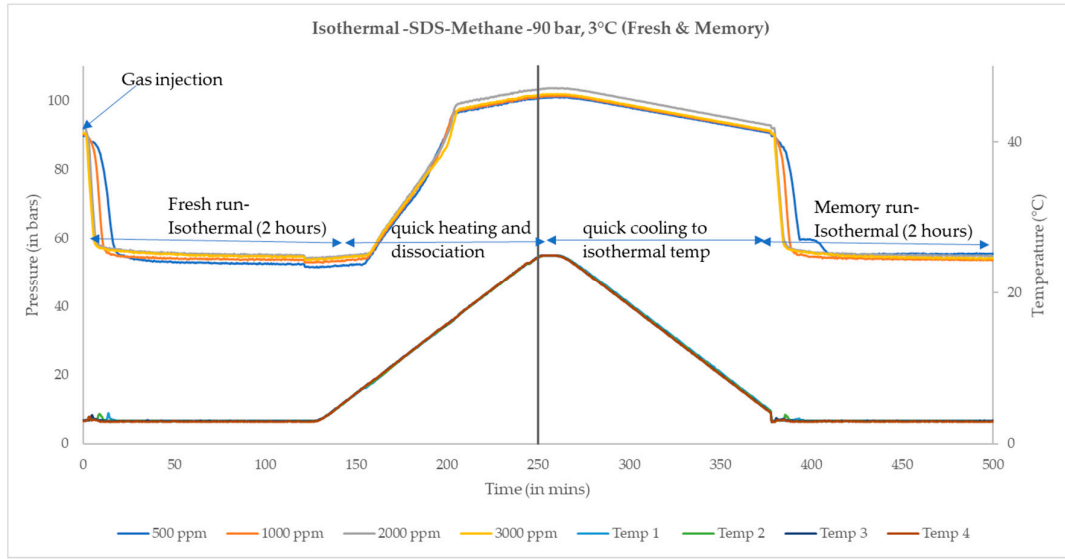
Figure 3. Graphical representation of typical identical isothermal experiments at 90 bar and 3 °C for different sodium dodecyl sulfate (SDS) concentrations (fresh and memory).

It is observed during the experiments that hydrate promoters bring more certainty into the system during the hydrate formation process, thus reducing the stochastic nature of hydrate formation. Only two repetition in each experiments are performed. According to Malcolm et al. [26], T_0 refers to the first macroscopic detection of hydrate formation, while T_a indicates the slow hydrate growth region before rapid hydrate formation, where the influence of SDS on hydrate behavior is minimal.

The difference between T_0 and T_a indicates the ability of SDS to influence rapid crystal growth after the first hydrate formation. Sub-cooling temperature (ΔT_{sub}) is a measure of the driving force, and it controls the hydrate growth curve. It can be expressed as the difference in T_{eq} and operational temperature T_{op} [27]. T_{op} is the temperature mostly referred to as the temperature during the isothermal test. In the equation above, T_{eq} is calculated using CSMGem software [28].

$$\Delta T_{sub} = T_{eq} - T_{op} \tag{1}$$

As explained before, T_0 is the temperature at which hydrate nucleation starts during constant temperature ramping. In a system containing hydrate promoters, an understanding of sub-cooling can be helpful to understand the effect of concentration increase of the same promoter in terms of the driving force. The maximum sub-cooling required in terms of hydrate nucleation in case of hydrate promoters can be expressed as

$$\Delta T_{sub} = T_{eq} - T_o \tag{2}$$

where T_0 is assumed to be T_{op} for the simplicity in the calculation.

Different sub-cooling for different concentrations in the case of SDS would refer to different operational requirements. Higher sub-cooling indicates the additional requirement for larger temperature drop below the hydrate equilibrium temperature for nucleation to start in case of methane hydrate.

Further, a change in sub-cooling is calculated by computing the difference between the sub-cooling temperature of pure water and sub-cooling temperature at a different concentration of SDS:

$$\Delta T_{sub,change} = \Delta T_{sub(purewater)} - \Delta T_{SDS,i} \tag{3}$$

$$\Delta T_{sub,change} = (T_{eq} - T_o)_{(purewater)} - (T_{eq} - T_o)_{SDS,i} \tag{4}$$

$$T_{eq,water} = T_{eq,SDS} \tag{5}$$

$$\Delta T_{sub,change} = T_{o(SDS,i)} - T_{o(purewater)} \tag{6}$$

$$\Delta T_{sub,change} < 0 \tag{7}$$

$\Delta T_{sub,change} < 0$ for SDS would indicate that the SDS-based system needs a higher degree of sub-cooling in comparison to a pure water-based system while forming methane hydrate. Additionally, results from isothermal experiments are generated as per Figures 3 above and Figure 4 below, which show the isothermal experiment at 90 bar and 3 °C for different SDS concentrations. The induction time t_0 has been defined as the time from the start of rocking to a first significant drop of pressure.

Catastrophic hydrate growth time (t_a) is defined as the time when the ball stops moving inside the cell, due to the formation of hydrate and represents the fastest growth region.
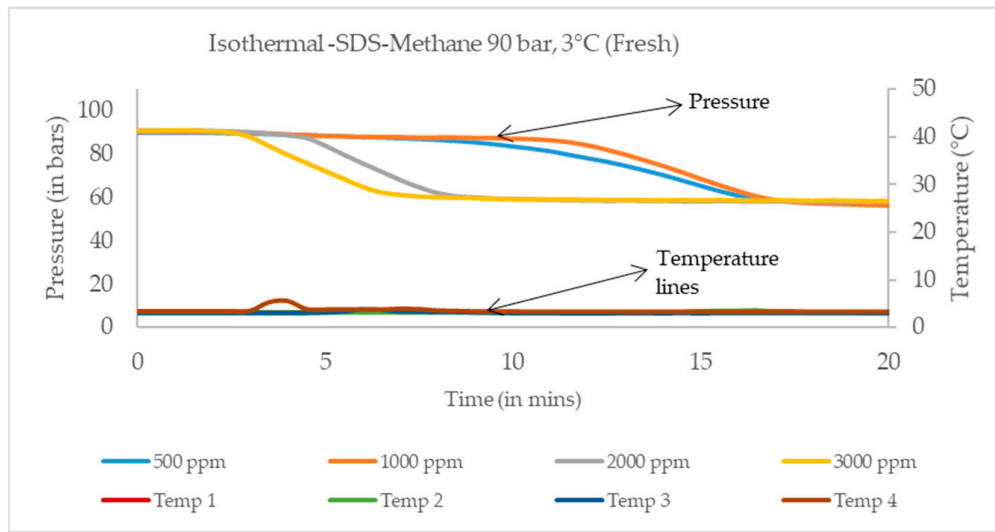

Figure 4. Graphical representation of isothermal experiments in shorter for different SDS concentrations with starting pressure 90 bar and T_{op}= 3 °C.

Standard examples to identify t_0 and t_a are described in Figure 5. A similar technique has been adapted previously by Astrid et al. [22]. According to Sloan et al. [29] the difference between ΔT_{sub} and ΔT_{op} provides the comparison of the operating temperature (isothermal tests) and expected onset temperature. The equation below provides a comparison between constant ramping and isothermal experiments.

$$\Delta T_{sub} - \Delta T_{op} = (T_{eq} - T_o) - (T_{eq} - T_{op}) = T_{op} - T_o \tag{8}$$

T_{eq} is constant by fixing the initial operating pressure for given SDS solution. If $T_{op} < T_0$, immediate hydrate formation is expected to occur. For the case when $T_{op} > T_0$, delay in hydrate formation is expected.

2.3.1. Hydrate Saturation

In general, methane hydrate formation can be represented by the following equation.

$$CH_4(g) + 6H_2O(l) \rightarrow CH_4.6H_2O(s)$$
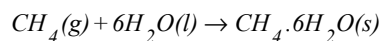
P–T data from isothermal experiments are used to study the hydrate saturation, and the total number of moles of CH_4 injected into the pressure cell is calculated as

$$nCH_{4,T} = \frac{P_1 V}{Z_1 RT} \tag{9}$$

P_1 is the initial operating pressure after methane gas is injected into the high-pressure cell, where $V (V = V_T - V_L)$ is the available gas volume in the reactor. V_T is the total cell volume and V_L is the SDS solution volume (equal to 10 mL). T is the temperature of the isothermal test. The compressibility factor Z_1 at given pressure and temperature is calculated using the Benedict-Webb-Rubin-Starling equation of state, R is the universal gas constant, 8.314 J·mol^{-1}·K^{-1}.

Assuming the process is a constant volume process, available gas volume remains constant after methane hydrate formation. $n_{CH4,H}$ is the number moles of methane in the gas phase after methane hydrate formation at the end of the experiment (2 h), and it is given by equation 10

$$n_{CH4,H} = \frac{P_2 V}{Z_2 RT} \tag{10}$$

where P_2 is the pressure at the end of 2 h, and Z_2 is the compressibility factor corresponding to P_2, T. The change in total number of moles of methane, $\Delta n_{CH4,H}$ trapped in methane hydrate formation is given by

$$\Delta n_{CH4,H} = \frac{P_1 V}{Z_1 RT} - \frac{P_2 V}{Z_2 RT} \tag{11}$$

The mass of the consumed solution in the methane hydrate formation m_c can be calculated as follows.

$$m_c = \Delta n_{CH4,H} N_H M_H \tag{12}$$

Here, M_H is the molar mass of water and N_H is the hydration number. N_H is considered constant for methane hydrate formation within the pressure range of 1.9 to 9.7 MPa and temperature range of 263 to 285 K. This gives an average hydration number that is CH$_4$-5.99 (± 0.07) H$_2$O, and 6.0 is used in these studies [30]. If the density of hydrate is 0.9 g/cm^3, the volume of hydrate is calculated as

$$V_H = \frac{m_c}{0.9} \tag{13}$$

and hydrate saturation can be calculated as

$$S_H = \frac{V_H}{V_L} \tag{14}$$

where V_L is the initial volume of the SDS solution, equal to 10 mL.

2.3.2. Normalized Gas Uptake

Normalized gas uptake, is calculated as the ratio of number of moles of methane gas captured in hydrate divided to the initial moles of the SDS solution, thus calculated as

$$n_{uptake} = \frac{\Delta n_{CH4,H}}{n_{SDS}} \tag{15}$$

Here, n_{SDS} is the moles of initial SDS solution. Additionally, the percentage of SDS solution consumed, $C_{SDSH} (\%)$ is determined from the equation as

$$C_{SDSH}\% = \frac{\Delta n_{CH_4,H} \times N_{Hyd}}{n_{SDS}} \times 100 \tag{16}$$

During the isothermal test, after the induction period, a period of linear growth is often observed, and this linear growth rate is quantified through a pressure drop rate K_p (s^{-1}) in the stable linear growth region. For this work, K_P is calculated, at the point of t_a and identified it as the point where we see a spike in the temperature profile.

$$Kp = \frac{dP^*}{dt} \tag{17}$$

P^* is the normalized pressure, since normalization mitigates small relative pressure differences between each cell. The growth profile is normalized by dividing the measured pressure P by the pressure recorded at the start of the test P_i.
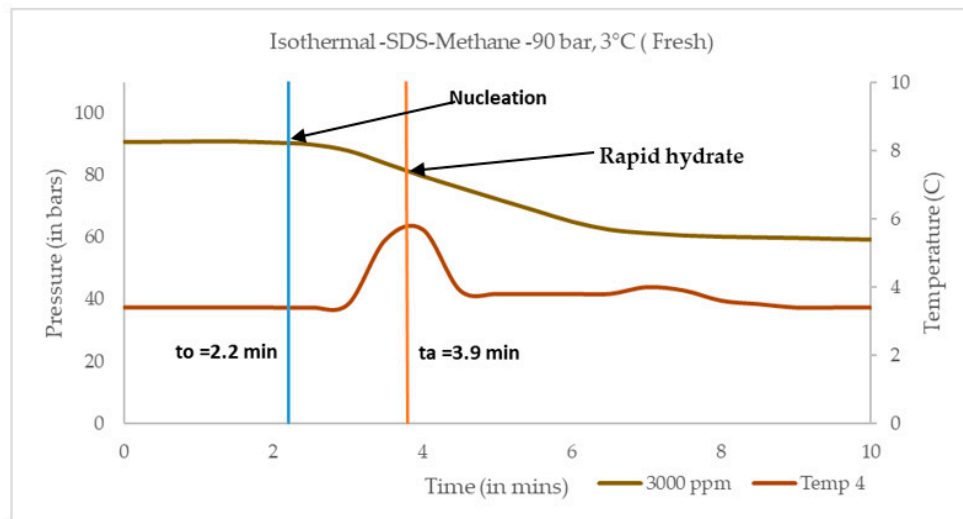
$$P^* = \frac{P}{P_i} \tag{18}$$

Figure 5. Graphical representation of the method adopted to demonstrate how to calculate t_o and t_a.

3. Results

Isothermal and constant ramping temperature schemes are applied to study the influence of different parameters, such as SDS concentration, rocking angle, solution volume, and different operating pressures on hydrate kinetics using rocking cell. Key parameters analyzed are onset of nucleation temperature, induction time, and normalized gas uptake.

3.1. Effect of Sample Volume and Rocking Angle (Fresh and Memory)

To fix the volume and rocking angle, we have tested three methods to study the effect of sample volume and rocking angle. These three methods are discussed in Table 1 which includes the different configuration tested for hydrate promoter. In method 1, the main parameter is the rocking angle of 35° and solution volume 10 mL, while method 2 and method 3 are indicative of more extreme cases causing pressure sensor blockage. For method 3, 20 mL and 40° angle resulted in blocking of the hydrate cell and a flat pressure line is observed. Therefore, angle reduction from 40° to 35° and volume reduction from 20 mL to 10 mL is chosen. Due to the blockage problems, method 2 and method 3 results could not be relied upon; hence, for all planned experiments, parameters selected

in method 1 are only considered. It can be concluded that at lower solution volume and lower rocking angle, hydrate promoter can be studied without causing blockage at the pressure sensor.

Table 2 summarizes the dataset of nucleation temperatures calculated at 90 bar methane pressure for fresh and memory samples at different SDS concentrations and under three different methods. Graphical representation of data based on Table 2 is described in Figure 6 to indicate the trend in T_0 for fresh sample as concentration changes.

Table 1. Summary of the three attempted methods and different rocking angle and solution volume configurations.

Method No	Rocking Angle	Solution Volume	Observation
Method 1	35°	10	No pressure sensor blockage
Method 2	35°	20	Pressure sensor blockage
Method 3	40°	20	Pressure sensor blockage

Table 2. Onset temperature T_o (°C) at 90 bar pressure and different sample volume and rocking angle.

	Method 1		Method 2		Method 3	
	10 mL/35°		20 mL/40°		20 mL/35°	
SDS conc (ppm)	Fresh T_o	Memory T_o	Fresh T_o	Memory T_o	Fresh T_o	Memory T_o
500	10.5	10.5	9.9	8.9	9.9	9.1
1000	10.3	9.95	8.9	9.3	8.9	8.9
2000	9.05	8.7	10	9	10	8.9
3000	9.2	9.8	9.8	8.4	9.8	9.2

In method 1, it is also evident that hydrate nucleation temperature T_0 is dependent on concentration, which becomes more evident in memory compared to the fresh solution.
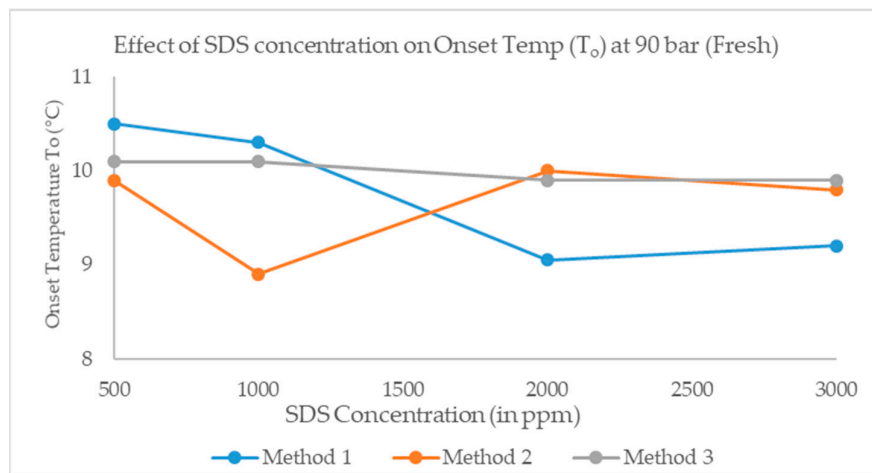

Figure 6. Onset temperature T_o versus SDS concentration for freshwater (method 1, method 2 and method 3).

3.2. The Onset of Nucleation Temperature (T_o) and Rapid Hydrate Formation Temperature (T_a) and Subcooling ΔT_{sub} for Constant Ramping Experiments

Rocking cell experiments are generally chosen for kinetic hydrate inhibitors (KHI). Hydrate formation in presence of KHI, is known to be stochastic. Currently, many KHI based publications using rocking cell reporting the T_0 based on 1–3 repetitions. Average values of T_0 and T_a are based on two trials. Percent deviation is only really meaningful if many trials are performed, say 8–10. The degree of sub cooling is also reported and discussed later in this section. The basis of the T_0

observation is that, T_o is determined where a sudden drastic slope change in the P–T curve is observed.

All concentrations of hydrate promoter give lower T_0 for SDS solutions compared to the pure water case. Therefore, $\Delta T_{sub,change} < 0$ for methane hydrate, formation in the presence of SDS compared to the pure water case, and nucleation starts at a lower temperature for SDS compared to pure water. Effect of concentration on T_0 is studied via constant ramping experiments. Results from the constant ramping experiment, including T_o for fresh and memory sample for methane hydrate formation, are summarized in Table 3 and graphical represented by Figure 7 According to Table 3, the effect of concentration on T_0 is not visible at lower pressures of 50 and 70 bar. As the pressure is increased above 70 bar, concentration starts to influence T_0. At higher pressure, as the concentration increases from 500 ppm to 2000 ppm, T_0 decreases to 2000 ppm while at 3000 ppm, it increases further. It means an increase in concentration delays the nucleation by lowering the nucleation temperature, and at higher concentration, the nucleation process starts at a lower temperature. The pressure is found to have the opposite effect and increases in pressure lead to an increase in the nucleation temperature at a constant concentration. It is clear from the figure that pure water has higher nucleation temperature compared to SDS-based systems at all pressures. At lower pressure, the difference between SDS and water-based methane hydrate promotion reduces.

Table 3. Onset of nucleation temperature T_0 (°C) vs. SDS concentration at different pressures from 50 bar to 120 bar.

SDS (in ppm)	120 bar		90 bar		70 bar		50 bar	
	Fresh	Memory	Fresh	Memory	Fresh	Memory	Fresh	Memory
0	13	13.2	10.5	10.8	8.4	8.6	5.45	5.5
500	12.6	13	10.5	10.5	8.1	8.2	5.3	5.3
1000	12.5	12.6	10.3	9.95	8	8.1	4.8	4.8
2000	10.4	11.2	9.05	8.7	7.6	7.7	4.7	4.7
3000	11.1	12.4	9.2	9.8	7.9	7.9	4.8	4.8

A change in the trend of nucleation temperature between 2000 ppm and 3000 ppm can be explained in terms of the existence of CMC for SDS solution between 2000 and 3000 ppm. Below the CMC, due to the presence of monomers, absorption decreases [14], which may have caused a delay in nucleation and lowering of the nucleation temperature compared to the pure water case. However, the trend is reversed above the CMC as absorption starts to increase due to micelle formation. Lee et al. [16], have also suggested that below the CMC, hydrate nucleation depends on monomer concentration.
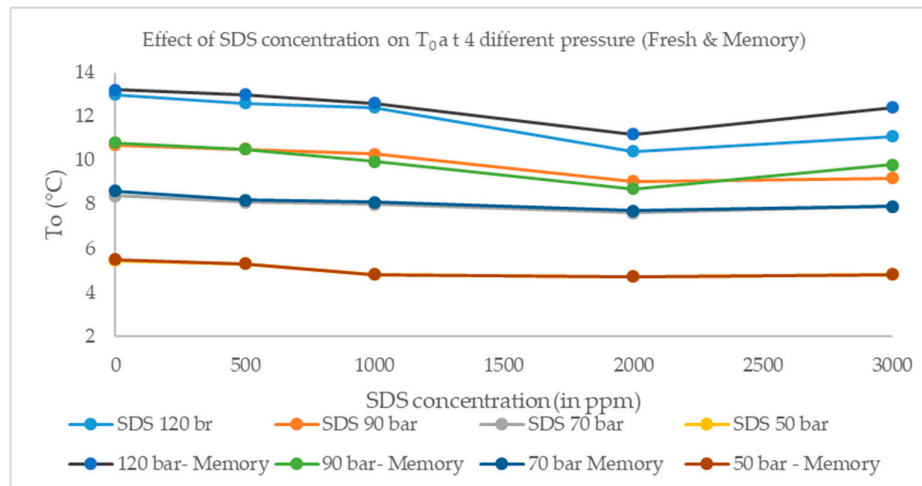

Figure 7. Effect of SDS concentration on T_o at different pressures both for fresh and memory run.

Comparing fresh and memory SDS samples, the memory sample follows a trend similar to the fresh sample at lower pressure; however, the deviation between fresh and memory is more visible at higher pressures. The difference in T_o observed for fresh and memory samples is wider at a higher pressure, which means the difference between fresh and memory SDS solution is more drastic at the higher-pressure range and for higher concentrations. From above, it can be said that T_0 is an absorption-dependent phenomenon, and the idea of CMC for SDS solutions is essential in the understanding of hydrate growth and kinetics.

During the constant cooling experiment, T_a was also studied and indicates the slow hydrate growth region before rapid hydrate formation. The difference between T_0 and T_a reflects the ability of the chemicals to hinder the rapid crystal growth of hydrates after nucleation begins [26]. Table 4 summarizes the difference between T_0 - T_a for the fresh SDS solution. Data from Table 4 are plotted in Figure 8 which indicate that as the concentration decreases, the influence of concentration upon hydrate growth rate decreases at all pressure values. At lower concentration, the higher initial operating pressure can to create higher driving force and control the hydrate growth profile. However, at higher concentrations, an increase in pressure is not able to accelerate the hydrate growth rate. Based on this, it can be said that a higher concentration of SDS, increase in the pressure would not affect the methane hydrate growth profile in the same order.

Table 4. Calculation of $T_0(°C)$, $T_a(°C)$, and $T_0 - T_a(°C)$ for fresh SDS Solution.

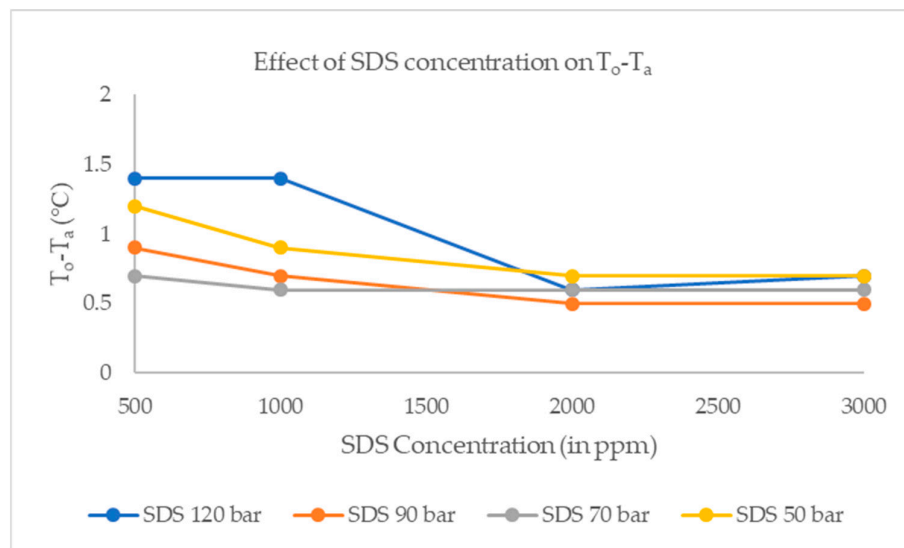|	120 bar			90 bar			70 bar			50 bar		
SDS (in ppm)	T_o	T_a	$T_o–T_a$	T_o	T_a	$T_o–T_a$	T_o	T_a	$T_o–T_a$	T_o	T_a	$T_o–T_a$
0	13.0	12.4	0.6	10.5	9.7	1.0	8.4	7.8	0.6	5.5	4.5	1.0
500	12.6	11.2	1.4	10.5	9.6	0.9	8.1	7.4	0.7	5.3	4.1	1.2
1000	12.5	11.0	1.4	10.3	9.6	0.7	8.0	7.4	0.6	4.8	3.9	0.9
2000	10.4	9.8	0.6	9.1	8.6	0.5	7.6	7.0	0.6	4.7	4.0	0.7
3000	11.1	10.4	0.7	9.2	8.7	0.5	7.9	7.3	0.6	4.8	4.1	0.7

Figure 8. $\Delta T_o–T_a$ at different pressure from 50–120 bar at different SDS concentration for fresh SDS solution.

Table 5 Summarizes the ΔT_{sub} from the constant ramping experiment, which is calculated according to $\Delta T_{sub} = T_{eq} - T_o$. The equilibrium temperature, T_{eq}, is calculated using CSMGem software for the pure water/methane system. SDS is a well-known kinetics promoter which does not affect the methane hydrate thermodynamics. Therefore, T_{eq} is considered the same for all concentrations of SDS at the same initial operating pressure. Looking at Figure 9, generated based on data from Table

5, it is evident that sub-cooling is dependent on both pressure and concentration. This driving force results in the observed growth profile, and indeed, all growth profiles are heavily influenced by the driving force. Although lower T_0 of the SDS system may indicate a delay in nucleation, but in fact it creates a higher driving force, compared to pure water even at lower SDS concentration. Hence, it reconfirms the positive effect of SDS on methane hydrate growth kinetics.

Table 5. Calculation of ΔT_{sub} and $\Delta T_{sub,change}$ for fresh SDS solution.

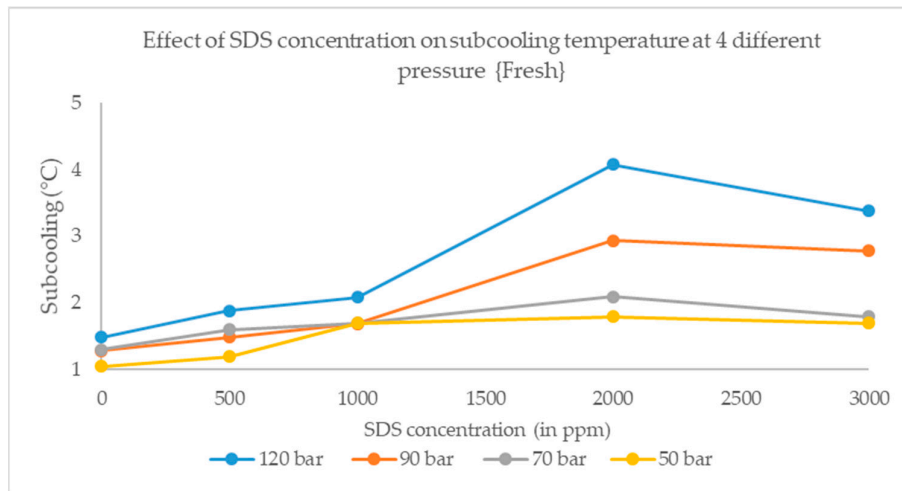| SDS (in ppm)	120 bars		90 bars		70 bars		50 bars	
	T_{eq}	14.479	T_{eq}	11.981	T_{eq}	9.691	T_{eq}	6.493
	ΔT_{sub}	$\Delta T_{sub,change}$	ΔT_{sub}	$\Delta T_{sub,change}$	ΔT_{sub}	$\Delta T_{sub,change}$	ΔT_{sub}	$\Delta T_{sub,change}$
0	1.479		1.481		1.291		1.043	
500	1.879	−0.4	1.481	−0.2	1.591	−0.3	1.193	−0.15
1000	1.979	−0.6	1.681	−0.4	1.691	−0.4	1.693	−0.65
2000	4.079	−2.6	2.931	−1.65	2.091	−0.8	1.793	−0.75
3000	3.379	−1.9	2.781	−1.5	1.791	−0.5	1.693	−0.65

Figure 9. Sub cooling temperature vs. SDS concentration at different pressures. This figure shows the presence of critical micelle concentration (CMC) in the range of 2000–3000 ppm concentration.

As the pressure increases, sub-cooling increases, as shown in Figure 9. Increase in sub-cooling is drastic between 1000 to 2000 ppm, while from 2000 to 3000 ppm it decreases due to an increase in T_0. The difference in absorption behavior above and below the CMC results in different sub-cooling, which is a key driving force for hydrate growth profile. Table 5 also summarizes the change in sub-cooling in the SDS system in comparison to pure water. Results confirmed that for the SDS-based system, $\Delta T_{sub,change} < 0$, which shows that SDS-based systems require cooling more than a water-based system to start nucleation of the methane hydrate, and this degree of cooling is further increased from 500 ppm to 2000 ppm, but decreases between 2000–3000 ppm.

3.3. Isothermal Experiments

With the aid of isothermal experiments, kinetics-based properties, such as induction time, methane hydrate storage capacity (gas uptake), and hydrate saturation are calculated. Table 6 summarizes the results from the isothermal experiments. For isothermal experiments, the driving force is quantified in terms of the difference in P_{eq} and P_{in} and influences the nucleation time of same system having different isothermal temperatures. Isothermal experiments have run for 2 h for SDS systems for the fresh sample case and is compared with pure water. It is found that no hydrates are formed in the pure water case at 90 bar, 3–5 °C temperature range, while hydrates are formed instantaneously in the case

of the SDS system. P_{eq} is calculated using CSMGem software for given operation temperatures, 3 °C and 5 °C. One of the patterns visible from Table 6 is that lower concentration delays the induction time; hence, it results in higher normalized gas uptake, hydrate saturation S_H, and water-to-hydrate conversation (X_{w-H}). In general, lower SDS concentrations act as inhibitors during the promotion while the higher concentration regime leads to hydrate promotion [31].

Table 6. Experimental results from isothermal experiments for fresh sample using rocking cell.

Exp.	SDS Conc.	Temp °C	P_{int}	P_{final}	Total Duration (min)	t_0 (min)	Driving Force (P_{in}-P_{eq})	n_{uptake} (mol)	S_H (%)	X_{W-H} %
1	500	5	89.9	54.0	120	4.75	47.00	0.114	75.77	68%
2	1000	5	90.5	55.0	120	4.25	47.57	0.114	75.83	68%
3	2000	5	90.5	56.8	120	3.50	47.62	0.109	72.83	66%
4	3000	5	90.5	56.0	120	2.75	47.60	0.111	74.04	67%
5	500	3	91.4	54.5	120	3.75	56.31	0.124	82.52	74%
6	1000	3	91.4	54.9	120	3.33	56.36	0.123	81.80	74%
7	2000	3	90.8	57.0	120	2.33	55.76	0.114	76.19	69%
8	3000	3	91.4	56.5	120	1.83	56.36	0.118	78.44	71%

Figure 10 is the plot between induction time and SDS concentration. Isothermal temperature is generally associated with operation temperature, and it can be represented as T_{op}. It is evident that as the concentration increases from 500 to 3000 ppm, induction time decreases from 4.75 min to 2.75 min at 5 °C and from 3.75 min to 1.83 min at 3 °C. At T_{op}= 5 °C, the driving force ($P_{in} - P_{eq}$) is ~47 bar, while at T_{op} = 3 °C, the driving force is ~56 bar. Thus, lowering the T_{op} leads to the higher driving force and lower induction time. Miller et al. [21] have discussed the crystallization kinetics of the SDS/H₂O system and concluded that a decrease in temperature increases both nucleation and growth rates. At constant T_{op}, increase in concentration leads to a decrease in induction time, valid for both 3 °C and 5 °C.
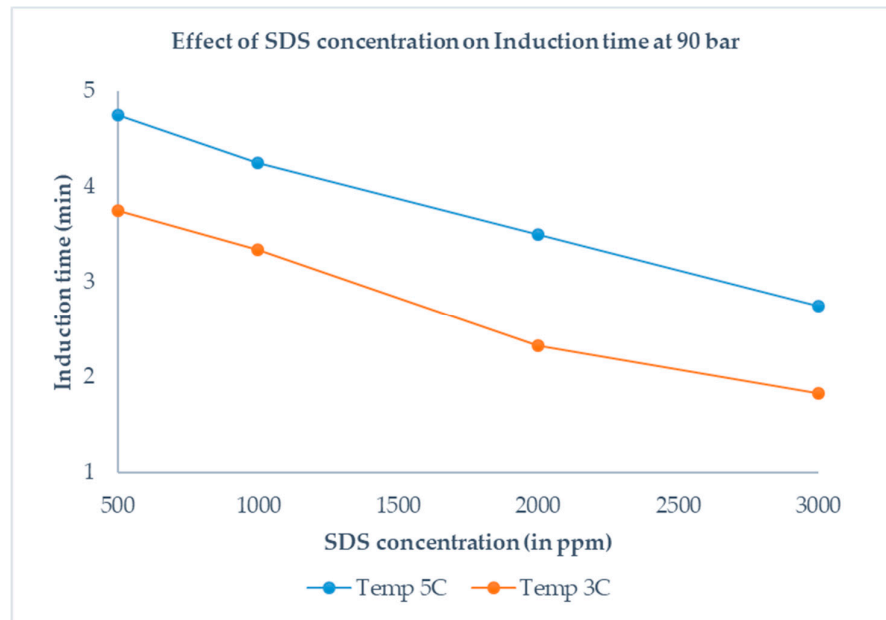

Figure 10. Induction time vs. SDS concentration at 3 °C and 5 °C for a fresh SDS sample. It can be seen that as concentration increases, induction time decrease.

Figure 11 highlights the correlation between normalized gas uptake and SDS concentration. It is evident that the normalized gas uptake is highest for 500 ppm. Figure 12 shows the variation in hydrate saturation vs. SDS concentration from isothermal experiments conducted with initial pressure 90 bar and operation temperatures of 3 °C and 5 °C. As the concentration increases, there is a decrease in hydrate saturation and 500 ppm SDS concentration is the optimal concentration for

hydrate saturation. The decrease in hydrate saturation can be explained as a decrease in absorption as concentration increases.
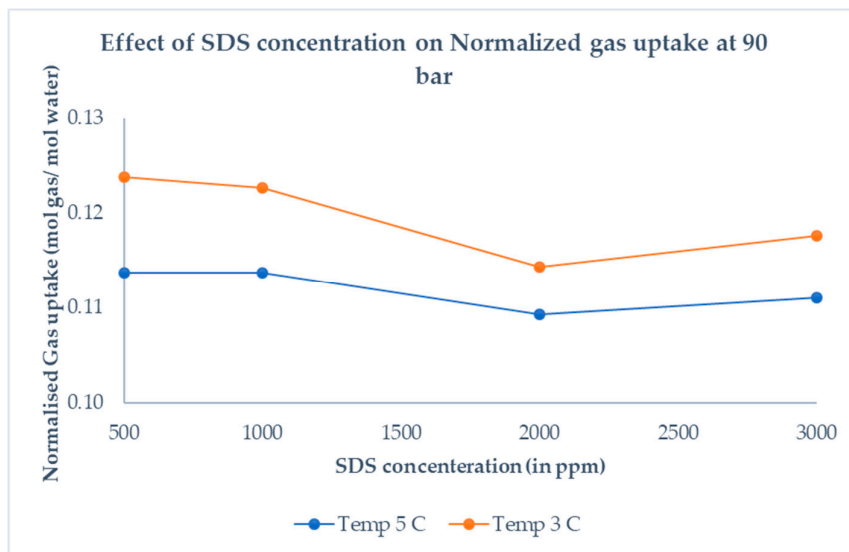

Figure 11. Normalized gas uptake vs. SDS concentration at 3 °C and 5 °C temperature for fresh SDS sample and initial pressure 90 bars. At the lower operating temperature, higher normalized gas uptake is observed, following a similar pattern of the hydrate saturation curve.
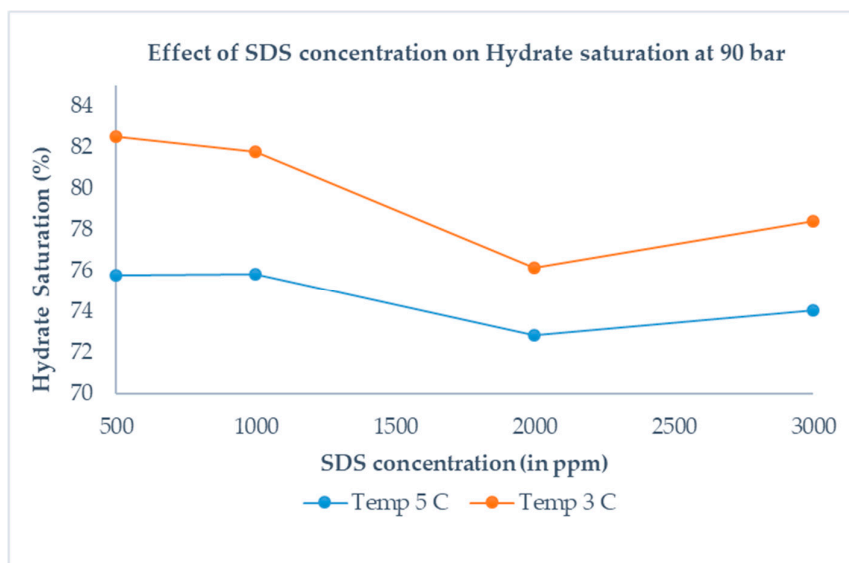

Figure 12. Hydrate saturation vs. SDS concentration at 3 °C and 5 °C for fresh sample and initial pressure of 90 bars. At lower operating temperature, higher hydrate saturation is observed, which changes around the expected CMC concentration.

By comparing Figures 11 and 12, it is evident that normalized gas uptake and hydrate saturation have similar trends. As the concentration increases, normalized gas uptake decreases, which leads to lower hydrate saturation.

Furthermore, Figures 10 and 11 provide evidence that the trend in induction time and normalized gas uptake are correlated. The higher the induction time, the higher is the gas uptake and thus higher is the hydrate saturation. Hence, it can be concluded that faster hydrate formation can be achieved at the cost of lower hydrate saturation when using surfactants like SDS. Therefore, there is

always a tradeoff in the decision for commercial-scale applications, where the choice to be made is between higher hydrate saturation and lower induction time.

Table 7 summarizes the different driving forces connected with T_0 ($T_0 - T_{op}$ and $T_{eq} - T_0$), induction time t_0, and K_p at 90 bar. Figure 13 shows the trend among $T_{eq} - T_0, T_0 - T_{op}$ and induction time t_0. It is evident that as the concentration increases, $T_{eq} - T_0$ (sub-cooling) increases while $T_0 - T_{op}$ decreases, which means sub-cooling acts as a driving force while $T_o - T_{op}$ acts as a resistant force. Figure 14 indicates a similar pattern for K_p concerning driving forces. It is also clear that K_p and t_0 complement each other, such that lowering the induction time t₀ leads to increase in K_p.

Table 7. $T_0 - T_{op}$ and $T_{eq} - T_0$ calculation based on isothermal and constant ramping experiments at constant pressure 90 bar.

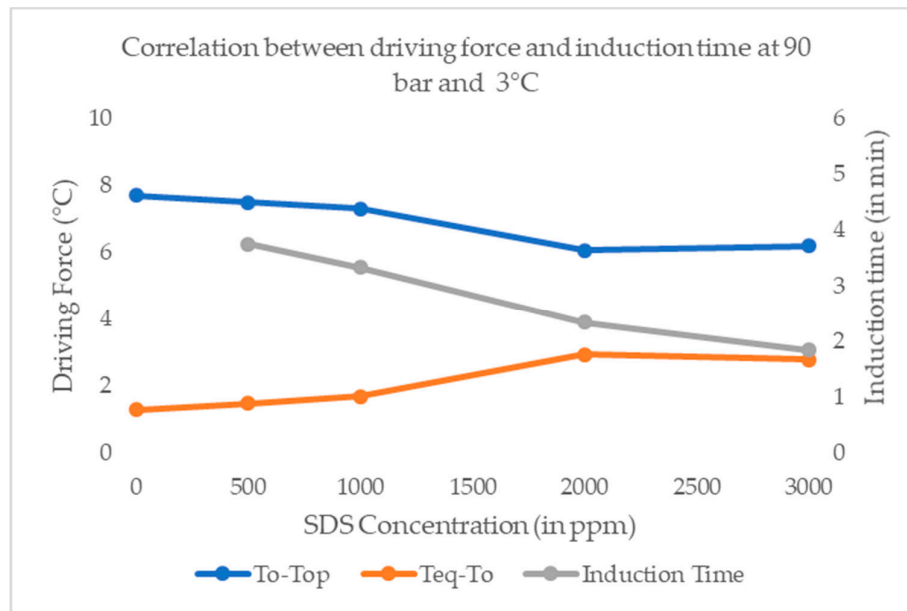| Exp | SDS (ppm) | Constant Ramping | Isothermal | Force | | Kinetics | |
		T_o (°C)	T_{op} (°C)	T_{eq}–T_o (°C)	T_o–T_{op} (°C)	Induction Time t₀ (min)	K_p (min⁻¹)
1	500	10.5	5	1.48	5.5	4.75	0.02
2	1000	10.3	5	1.68	5.3	4.25	0.04
3	2000	9.05	5	2.93	4.1	3.50	0.06
4	3000	9.2	5	2.78	4.2	2.75	0.07
5	500	10.5	3	1.48	7.5	3.75	0.04
6	1000	10.3	3	1.68	7.3	3.33	0.04
7	2000	9.05	3	2.93	6.1	2.33	0.05
8	3000	9.2	3	2.78	6.2	1.83	0.09

Figure 13. Correlation between driving force and induction time for T_{op} = 3 °C. Induction time varies with different driving forces in isothermal and constant ramping temperature schemes.
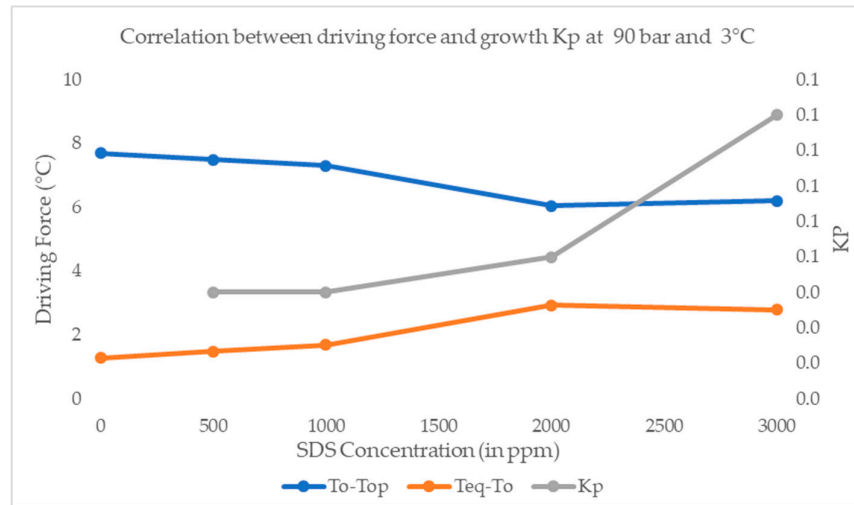
Figure 14. Driving forces vs. growth K_p for T_{op} = 3 °C, Growth K_p varies with different driving forces in isothermal and constant ramping temperature schemes.

3.4. Proposed Hypothesis

The mechanism with which surfactants like SDS affect methane hydrate promotion is not well agreed upon, and many potential theories have been proposed to explain the hydrate promotion behavior above and below the CMC [18]. Key mechanisms behind surfactant role as hydrate promoter are interfacial energy, absorption, and CMC. However, there is no consensus among researchers about exact mechanism responsible for hydrate promotion behavior. Based on the results of this work, our hypothesis is based on the role of absorption and surface tension. Figures 15 and 16 highlight the hypothesis derived from the interplay between absorption and surface tension and their effects on onset temperature, gas uptake and induction time. Based on our experimental data, we hypothesize that gas uptake and onset temperature is an absorption-dependent phenomenon and follows the absorption trend along with the CMC value. This results in the finding that below the CMC, absorption and gas uptake decrease, and the opposite is true above the CMC.
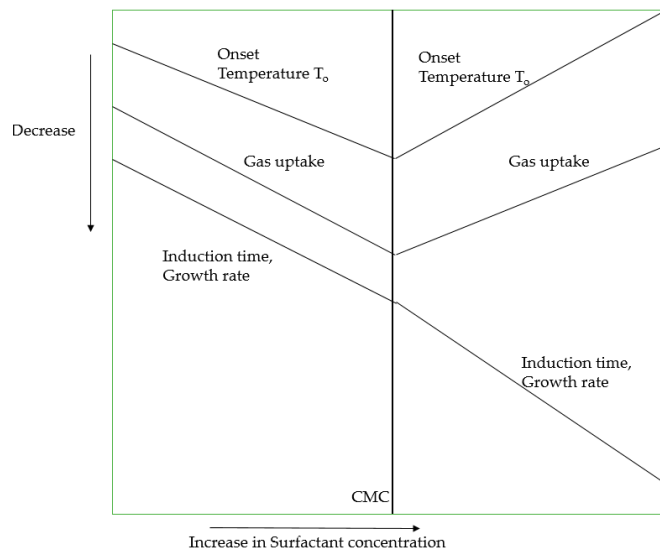

Figure 15. Summary of the trend observed in key properties including onset temperature, gas uptake and induction time as surfactant concentration increases. Summarize results confirm the presence of CMC between 2000–3000 ppm around which change in trend is observed.
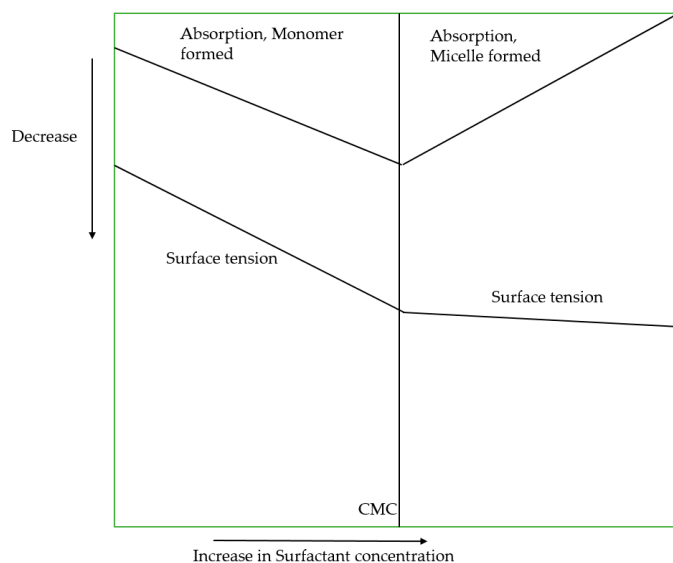
Figure 16. Trend in key active mechanism applied in surfactant to understand the effect of SDS concentration.

Another proposition is that a decrease in induction time is a surface tension-dependent phenomenon. Increase in SDS concentration until the CMC value, correlate well with decrease in surface tension and decrease in the induction time at a given temperature. Sun et al. [32] have shown that for methane + water system, interfacial tension decrease drastically with addition of SDS below CMC and surface tension value remain constant above CMC value. Therefore, decrease in induction time above CMC value can be attributed to increase in the absorption or creation of micelles.

4. Conclusions

This study show that rocking cell setup can be a useful experimental technique to study the hydrate promoter performance at appropriate sample volume and rocking angle. Experimental results suggest that the onset of nucleation temperature is dependent on the concentration of SDS, which is a critical parameter that affects methane hydrate growth kinetics. There is a tradeoff between growth kinetics and normalized gas uptake when selecting the optimal concentration of SDS. A higher concentration of SDS leads to lower induction time, while lower concentration leads to higher normalized gas uptake and higher hydrate saturation. According to the proposed framework, absorption controls the gas uptake, while surface tension controls the induction time below the CMC. Absorption and surface tension both are dependent on the CMC of SDS, and there is a change in the pattern below and above the CMC.

Author Contributions: Conceptualization, methodology, investigation, writing-original draft preparation, and review and editing: J.S.P.; Formal analysis, investigation: Y.J.D.; Review and editing, supervision, project administration, and funding acquisition: N.v.S.

Reference

1. Veluswamy, H.P.; Kumar, A.; Seo, Y.; Lee, J.D.; Linga, P. A review of solidified natural gas (SNG) technology for gas storage via clathrate hydrates. *Appl. Energy* **2018**, *216*, 262–285.
2. Sadeq, D.; Iglauer, S.; Lebedev, M.; Smith, C.; Barifcani, A. Experimental determination of hydrate phase equilibrium for different gas mixtures containing methane, carbon dioxide and nitrogen with motor current measurements. *J. Nat. Gas Sci. Eng.* **2017**, *38*, 59–73.
3. Pan, Z.; Liu, Z.; Zhang, Z.; Shang, L.; Ma, S. Effect of silica sand size and saturation on methane hydrate formation in the presence of SDS. *J. Nat. Gas Sci. Eng.* **2018**, *56*, 266–280.
4. Chong, Z.R.; Yang, S.H.B.; Babu, P.; Linga, P.; Li, X. Sen Review of natural gas hydrates as an energy resource: Prospects and challenges. *Appl. Energy* **2016**, *162*, 1633–1652.
5. Pandey, J.S.; Solms, N. von Hydrate Stability and Methane Recovery from Gas Hydrate through CH4–CO2 Replacement in Different Mass Transfer Scenarios. *Energies* **2019**, *12*, 2309.
6. Jensen, L.; Thomsen, K.; Solms, N. Von Inhibition of Structure I and II Gas Hydrates using Synthetic and Biological Kinetic Inhibitors. *Energy & Fuels* **2011**, *25*, 17–23.
7. Brown, T.D.; Taylor, C.E.; Bernardo, M.P. Rapid Gas Hydrate Formation Processes: Will They Work? *Energies* **2010**, *3*, 1154–1175.
8. Sadeq, D.; Alef, K.; Iglauer, S.; Lebedev, M.; Barifcani, A. Compressional wave velocity of hydrate-bearing bentheimer sediments with varying pore fillings. *Int. J. Hydrogen Energy* **2018**, *43*, 23193–23200.
9. Okutani, K.; Kuwabara, Y.; Mori, Y.H. Surfactant effects on hydrate formation in an unstirred gas / liquid system: An experimental study using methane and sodium alkyl sulfates. *Chem. Eng. Sci.* **2008**, *63*, 183–194.
10. Zhong, Y.; Rogers, R.E. Surfactant effects on gas hydrate formation. *Chem. Eng. Sci.* **2000**, *55*, 4175–4187.
11. Schramm, L.L.; Stasiuk, E.N.; Marangoni, D.G. Surfactants and their applications. *Annu. Rep. Prog. Chem. Sect. C* **2003**, *99*, 3–48.
12. Zhang, J.S.; Lee, S.; Lee, J.W. Solubility of sodium dodecyl sulfate near propane and carbon dioxide hydrate-forming conditions. *J. Chem. Eng. Data* **2007**, *52*, 2480–2483.
13. Song, J.H.; Couzis, A.; Lee, J.W. Investigation of macroscopic interfacial dynamics between clathrate hydrates and surfactant solutions. *Langmuir* **2010**, *26*, 18119–18124.
14. Demissie, H.; Duraisamy, R. Effects of electrolytes on the surface and micellar characteristics of Sodium dodecyl sulphate surfactant solution. *J. Sci. Innov. Res.* **2016**, *5*, 208–214.
15. Yoslim, J.; Linga, P.; Englezos, P. Enhanced growth of methane—propane clathrate hydrate crystals with sodium dodecyl sulfate, sodium tetradecyl sulfate, and sodium hexadecyl sulfate surfactants. *J. Cryst. Growth* **2010**, *313*, 68–80.
16. Zhang, J.S.; Lee, S.; Lee, J.W. Kinetics of Methane Hydrate Formation from SDS Solution. *Ind. Eng. Chem. Res.* **2007**, 6353–6359.
17. Liu, W.; Li, Y.; Xu, X. Influence factors of methane hydrate formation from ice: Temperature, pressure and SDS surfactant. *Chin. J. Chem. Eng.* **2019**, *27*, 405–410.
18. Kumar, A.; Bhattacharjee, G.; Kulkarni, B.D.; Kumar, R. Role of Surfactants in Promoting Gas Hydrate Formation. *Ind. Eng. Chem. Res.* **2015**, *54*, 12217–12232.
19. Naeiji, P.; Varaminian, F. Differential scanning calorimetry measurements and modeling of methane + THF hydrate growth kinetics based on non-equilibrium thermodynamics. *J. Mol. Liq.* **2018**, *263*, 22–30.
20. Mcnamee, K.P. Evaluation of Kinetic Hydrate Inhibitor Performance by High-Pressure Differential Scanning Calorimetry. In Proceedings of the Offshore Technology Conference, Houston, TX, USA, 2–5 May 2011.
21. Miller, R.M.; Poulos, A.S.; Robles, E.S.J.; Brooks, N.J.; Ces, O.; Cabral, J.T. Isothermal Crystallization Kinetics of Sodium Dodecyl Sulfate-Water Micellar Solutions. *Cryst. Growth Des.* **2016**, *16*, 3379–3388.
22. Lone, A.; Kelland, M.A. Exploring kinetic hydrate inhibitor test methods and conditions using a multicell steel rocker rig. *Energy Fuels* **2013**, *27*, 2536–2547.
23. Sa, J.-H.; Melchuna, A.; Zhang, X.; Morales, R.E.M.; Cameirão, A.; Herri, J.-M.; Sum, A.K. Rock-Flow Cell: An Innovative Benchtop Testing Tool for Flow Assurance Studies. *Ind. Eng. Chem. Res.* **2019**, *58*, 8544–8552.
24. Daraboina, N.; Pachitsas, S.; Von Solms, N. Experimental validation of kinetic inhibitor strength on natural gas hydrate nucleation. *Fuel* **2015**, *139*, 554–560.
25. Daraboina, N.; Von Solms, N. The combined effect of thermodynamic promoters tetrahydrofuran and cyclopentane on the kinetics of flue gas hydrate formation. *J. Chem. Eng. Data* **2015**, *60*, 247–251.

26. Kelland, M.A.; Abrahamsen, E.; Ajiro, H.; Akashi, M. Kinetic Hydrate Inhibition with N-Alkyl-N-vinylformamide Polymers: Comparison of Polymers to n-Propyl and Isopropyl Groups. *Energy Fuels* **2015**, *29*, 4941–4946.

27. Kelland, M.A. History of the development of low dosage hydrate inhibitors. *Energy Fuels* **2006**, *20*, 825–847.

28. Sloan, E.D.; Koh, C.A.; Koh, C. *Clathrate Hydrates of Natural Gases*, 3rd ed.; CRC Press: Boca Raton, FL, USA, 2007.

29. Sloan, E.D.; Subramanian, S.; Matthews, P.N.; Lederhos, J.P.; Khokhar, A.A. Quantifying hydrate formation and kinetic inhibition. *Ind. Eng. Chem. Res.* **1998**, *37*, 3124–3132.

30. Yoon, J.; Kawamura, T.; Yamamoto, Y.; Komai, T. Transformation of Methane Hydrate to Carbon Dioxide Hydrate: In Situ Raman Spectroscopic Observations. *J. Phys. Chem. A* **2004**, *108*, 5057–5059.

31. Nguyen, N.N.; Nguyen, A.V.; Dang, L.X. The inhibition of methane hydrate formation by water alignment underneath surface adsorption of surfactants. *Fuel* **2017**, *197*, 488–496.

Sun, C.Y.; Chen, G.J.; Yang, L.Y. Interfacial tension of methane + water with surfactant near the hydrate formation conditions. *J. Chem. Eng. Data* **2004**, *49*, 1023–1025.